Chemical Engineering Journal 96 (2003) 71–80

Chemical Engineering Journal

www.elsevier.com/locate/cej

CFD simulation of concurrent-up gas–solid flow in circulating fluidized beds with structure-dependent drag coefficient

Ning Yang*, Wei Wang, Wei Ge, Jinghai Li

Multi-phase Reaction Laboratory, Institute of Process Engineering, Chinese Academy of Sciences, P.O. Box 353, Beijing 100080, PR China

Abstract

Meso-scale structure existing in the form of particle clusters or strands in concurrent-up gas–solid two-phase flow has been extensively corroborated in experimental research. However, its significant effects on interfacial drag coefficient are seldom taken into account in current computational fluid dynamic (CFD) simulations by using the two-fluid models. The energy-minimization multi-scale (EMMS) approach, in which the heterogeneous structure is described by the so-called multi-scale resolution and energy-minimization method, is adapted in this study for investigating the dependence of drag coefficient on structure parameters. The structure-dependent drag coefficients calculated from the EMMS approach are then incorporated into the two-fluid model to simulate the behavior of the concurrent-up gas–solid flow in a riser. Simulation results indicate that the simulated solid concentration with the Wen and Yu/Ergun drag correlations is rather dilute, leading to a more homogenous structure; while the dynamic formation and dissolution of clusters can be captured with the drag correlations derived from the EMMS approach, and the simulated outlet solid flux and voidage profile in both radial and axial directions are in reasonable agreement with experimental results, suggesting the feasibility for the EMMS approach to be used as a sub-grid closure law for drag coefficient.

Keywords: CFD simulation; Drag coefficient; Gas–solid flow; Two-fluid model; Multi-scale; Fluidization

1. Introduction

Most chemical processes involving gas–solid two-phase flow, such as fluid catalytic cracking (FCC) and circulating fluidized bed combustion (CFBC), are essentially non-linear and non-equilibrium with the so-called *multi-scale* structure as their common nature [1]. For example, the CFB systems usually operate under the regime of fast fluidization with higher flow rate of gas and solid, and lower diameter and density of particles, leading to more intensive gas–particle interaction and therefore more heterogeneous flow structure characterized by dynamic formation and dissolution of strands or clusters on the meso-scale, and a dilute-top/dense-bottom and dilute-core/dense-wall structure in a macro sense.

Apart from experimental investigation, recent years have seen a rapid growth of computer simulation of gas–solid two-phase flow. Most of these simulations are based on the two-fluid approach in which gas and solid are assumed to be continuous and fully interpenetrating in each control volume, so the conservative equations of mass and momentum originally derived from single-phase flow can be extended to describe the hydrodynamics of gas–solid two-phase flow [2–4]. Among others, the most important and arguable are the constitutive correlations for the solid stress and the interfacial drag coefficient. If the stress–strain relationship for solid phase is represented by a Newtonian form as that for gas phase, correlations should be established for the so-called solid "pressure" and "viscosity". In some previous works [3–5], various forms of empirical correlations for the solid pressure were proposed based on the data from powder compaction experiments, and the solid viscosity was ignored, or assumed to be a constant or some simple functions of the solid volume fraction. In recent years, a first principle method called kinetic theory for granular flow (KTGF), originating from the theory for the non-uniform dense gases described by Chapman and Cowling [6], has been developed to establish the constitutive correlations for solid pressure and viscosity [7,8].

While much attention has been focused on establishing the appropriate correlations for solid stress, little effort is made to the interfacial drag coefficient, which is usually modified from single particle drag coefficient by a correction factor proposed by Wen and Yu [9] or Ergun [10]. These correlations were originally derived from the experimental results for homogeneous systems such as particulate fluidized beds or fixed beds. However, the flow structure is

* Corresponding author. Fax: +86-10-62558065.
E-mail address: nyang@home.ipe.ac.cn (N. Yang).

1385-8947/$ – see front matter © 2003 Elsevier B.V. All rights reserved.
doi:10.1016/j.cej.2003.08.006

Nomenclature

a	acceleration of particles ($m\,s^{-2}$)
C_{Dc}	drag coefficient for a particle in dense phase (–)
C_{Df}	drag coefficient for a particle in dilute phase (–)
C_{Di}	drag coefficient for a cluster (–)
C_{D0}	standard drag coefficient for a particle (–)
d_{cl}	cluster diameter (m)
d_p	particle diameter (m)
f	volume fraction of dense phase (–)
g	gravity acceleration ($m\,s^{-2}$)
G_s	solid flow rate ($kg\,m^{-2}\,s^{-1}$)
N_T	mass specific total energy consumption for particles ($W\,kg^{-1}$)
N_{st}	mass specific energy consumption for suspending and transporting particles ($W\,kg^{-1}$)
$\bar{u}_k$	$k = g, p$, gas or solid velocity tensor ($m\,s^{-1}$)
U_c	superficial fluid velocity in dense phase ($m\,s^{-1}$)
U_f	superficial fluid velocity in dilute phase ($m\,s^{-1}$)
U_g	superficial fluid velocity ($m\,s^{-1}$)
U_{mf}	superficial fluid velocity at minimum fluidization ($m\,s^{-1}$)
U_p	superficial particle velocity ($m\,s^{-1}$)
U_{pc}	superficial particle velocity in dense phase ($m\,s^{-1}$)
U_{pf}	superficial particle velocity in dilute phase ($m\,s^{-1}$)
U_s	superficial slip velocity ($m\,s^{-1}$)
U_{sc}	superficial slip velocity in dense phase ($m\,s^{-1}$)
U_{sf}	superficial slip velocity in dilute phase ($m\,s^{-1}$)
U_{si}	superficial slip velocity in inter-phase ($m\,s^{-1}$)

Greek symbols

β	drag coefficient for a control volume ($kg\,m^{-3}\,s^{-1}$)
β_0	see Eq. (13) for definition ($kg\,m^{-3}\,s^{-1}$)
ε_c	voidage of dense phase (–)
ε_f	voidage of dilute phase (–)
ε_{max}	maximum voidage for particle aggregating (0.9997) (–)
ε_{mf}	voidage at minimum fluidization (–)
ε_k	$k = g, p$, gas or solid volume fraction (–)
μ_k	$k = g, p$, gas or solid viscosity (Pa s)
ρ_g	fluid density ($kg\,m^{-3}$)
ρ_p	solid density ($kg\,m^{-3}$)
$\bar{\bar{\tau}}_k$	$k = g, p$, gas or solid stress tensor ($N\,m^{-2}$)
ω	see Eq. (14) for definition (–)

Subscripts

g	gas phase
p	solid phase

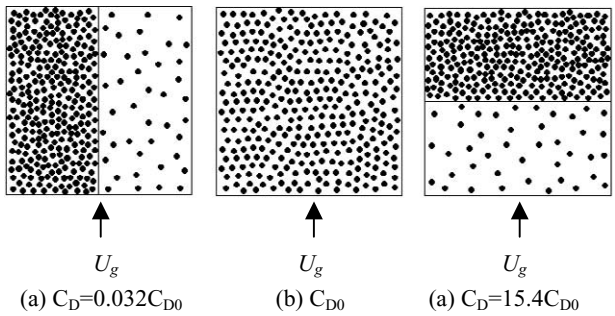

Fig. 1. Effects of simplified flow structure on drag coefficient with the same amount of particles and the same gas flow rate (FCC/air: $d_p = 54\,\mu m$, $\rho_p = 930\,kg\,m^{-3}$, $U_g = 0.01\,m\,s^{-1}$, $\varepsilon_c = 0.48$, $\varepsilon_f = 0.96$, $f = 0.5$).

definitely heterogeneous in gas–solid fluidization even at a scale as small as the control volume of computational fluid dynamics (CFD) [11]. In fact, the clustering nature of the CFB system, as evidenced by the tendency of particles to aggregate while interacting with gas, has been utilized to explain the large gas–solid slip velocity found in experimental research. Therefore, the validity of these correlations for heterogeneous gas–solid systems is quite questionable.

It is noticed that some researchers have found that the drag coefficient was a key parameter for the simulation of CFB systems. Li et al. [12] pointed out that the drag coefficients based on average approaches were inadequate to represent the gas–solid contacting in CFB systems, and their further investigation on three cases of simplified flow structure, as shown in Fig. 1, revealed the significant dependence of drag coefficient on structural changes [13]. O'Brien and Syamlal [14] found that the drag correlations must be corrected to account for cluster formation for fine particles, and claimed that the unphysical adjustment of the solid stress was not the correct approach. Qi et al. [15] reported that the particles fed into the riser got elutriated immediately, and the simulated flow became rather dilute as a whole if the drag correlation derived from Ergun equation was employed. They claimed that the current drag correlations were only suitable for low gas velocity and coarse particles, in which case the terminal velocity was equal or close to the superficial gas velocity. Agrawal et al. [16] further reported that the contribution of solid stress obtained from KTGF was negligible, and the effect of particle clusters played a dominant role in their simulation.

These questions imply that the drag coefficient for a control volume is strongly dependent on the meso-scale structure, leading us to investigate the relationship between drag coefficient and the meso-scale structure parameters. In our previous work [17], the energy-minimization multi-scale (EMMS) approach was modified to investigate the variation of structure parameters with solid concentration, showing the tendency for particles to aggregate to form clusters and for fluid to pass around clusters. The objective of this study is to extend our previous work [18] and to further employ this approach to calculate the drag coefficient from

structure parameters, and incorporate it into the two-fluid model. Comparisons of the simulation results between this new approach and the Wen and Yu/Ergun drag correlations are carried out to demonstrate its effectiveness.

2. Calculation of structure-dependent drag coefficient

2.1. Mathematical model

The original model proposed by Li and Kwauk [19] was for describing the flow structure of a global fluidized bed system, and we now extend its principle to the control volume of the two-fluid model. In each control volume, gas and particles are considered to be either in the particle-rich dense phase or in the gas-rich dilute phase. The mechanisms of gas–solid interactions should be analyzed for different scales: the interaction between a single particle and the nearby fluid inside both the dense and dilute phases (micro-scale), and the interaction between clusters and the surrounding dilute broth (meso-scale). Eight phase-specific parameters are proposed to describe the flow structure and the mechanisms of gas–solid interactions, i.e., ε_f, U_f and U_{pf} for the dilute phase, and ε_c, U_c, U_{pc}, f, and d_{cl} for the dense phase. In order to establish the mathematical model, the following assumptions are adopted:

- The dense phase exists as spherical clusters and its minimum voidage is ε_{mf}.
- Only drag and gravity are considered, and other forces are neglected.
- The distribution of particles inside the dense phase and dilute phase, and the distribution of clusters in a control volume are homogeneous, so the correlation of Wen and Yu can be used for particles inside each phase and for clusters in the so-called inter-phase, i.e., the "phase" between the dense clusters and the dilute broth.

Compared with the original model [19] in which the drag force is assumed to be balanced with gravity, the model in this paper takes the average acceleration for particles in a control volume into consideration. The mathematical model can then be formulated as the following set of non-linear equations:

- Momentum equation for particles in the dense phase:

$$\frac{3}{4}C_{Dc}\frac{f(1-\varepsilon_c)}{d_p}\rho_g U_{sc}^2 + \frac{3}{4}C_{Di}\frac{f}{d_{cl}}\rho_g U_{si}^2 = f(1-\varepsilon_c)(\rho_p-\rho_g)(g+a) \quad (1)$$

- Momentum equation for particles in the dilute phase:

$$\frac{3}{4}C_{Df}\frac{1-\varepsilon_f}{d_p}\rho_g U_{sf}^2 = (1-\varepsilon_f)(\rho_p-\rho_g)(g+a) \quad (2)$$

- Momentum equation for all the particles:

$$\frac{\beta}{\varepsilon_g}\frac{U_s}{\varepsilon_g} = (1-\varepsilon_g)(\rho_p-\rho_g)(g+a) \quad (3)$$

where β represents the drag coefficient for a control volume (type A, see [8]), and U_s represents the superficial slip velocity:

$$U_s = U_g - \frac{G_s\varepsilon_g}{\rho_p(1-\varepsilon_g)} \quad (4)$$

- Pressure balance between the dense phase and the dilute phase:

$$C_{Df}\frac{1-\varepsilon_f}{d_p}\rho_g U_{sf}^2 + \frac{f}{1-f}C_{Di}\frac{1}{d_{cl}}\rho_g U_{si}^2 = C_{Dc}\frac{1-\varepsilon_c}{d_p}\rho_g U_{sc}^2 \quad (5)$$

- Mass balance of gas and particles:

$$U_g = fU_c + (1-f)U_f \quad (6)$$

$$U_p = fU_{pc} + (1-f)U_{pf} \quad (7)$$

- Cluster diameter [19]:

$$d_{cl} = \frac{d_p[U_p/(1-\varepsilon_{max}) - (U_{mf} + U_p\varepsilon_{mf}/(1-\varepsilon_{mf}))]g}{N_{st}\rho_p/(\rho_p-\rho_g) - (U_{mf} + U_p\varepsilon_{mf}/(1-\varepsilon_{mf}))g} \quad (8)$$

- Overall voidage:

$$\varepsilon_g = \varepsilon_c f + \varepsilon_f(1-f) \quad (9)$$

The relevant parameters in these equations are summarized in the nomenclature. There are totally 10 variables (U_f, U_{pf}, U_c, U_{pc}, ε_c, ε_f, f, d_{cl}, β, a) and eight independent equations, i.e., Eqs. (1)–(3) and (5)–(9) in the model, calling for evoking the stability condition to close the equations, i.e., the minimization of the portion for energy consumption N_{st} with respect to the total energy N_T, as shown below:

$$\frac{N_{st}}{N_T} = \frac{U_g(1-\varepsilon_g) - fU_f(\varepsilon_f-\varepsilon_g)(1-f)}{U_g(1-\varepsilon_g)} = \min. \quad (10)$$

where

$$N_{st} = \left[U_g - \frac{\varepsilon_f-\varepsilon_g}{1-\varepsilon_g}f(1-f)U_f\right](g+a)\frac{\rho_p-\rho_g}{\rho_p} \quad (11)$$

$$N_T = \frac{\rho_p-\rho_g}{\rho_p}U_g(g+a) \quad (12)$$

The definition of energy terms and stability condition was proposed in the work of Li and Kwauk [19]. Here the stability condition is used to search for the right solution of structure parameters by minimizing the energy consumption. In summary, with the specified operating conditions (U_g, G_s), the overall voidage (ε_g), and the material properties (ρ_g, ρ_p, d_p, μ_g), the eight structure parameters (U_f, U_{pf}, U_c, U_{pc}, ε_c, ε_f, f, d_{cl}), the acceleration term (a) and the drag coefficient for a control volume (β) can be obtained by solving the above non-linear optimization problem.

2.2. Calculation of drag coefficient

It can be observed that the drag coefficient is correlated with the structure parameters by the non-linear equations, implying that it can be regarded as an implicit function of structure parameters. In this manner, the relationship between structure parameters and drag coefficient is established in our model. We denote β_0 as the standard drag coefficient without consideration of the effect of neighboring particles, i.e.:

$$\beta_0 = \frac{3}{4}\frac{1-\varepsilon_g}{d_p}\rho_g U_s C_{D0} \tag{13}$$

where C_{D0} denotes the standard drag coefficient for an individual particle. Then, we denote ω as the correction factor for drag coefficient:

$$\omega = \frac{\beta}{\beta_0} \tag{14}$$

Upon some simple manipulations, the correction factor of Wen and Yu's correlation can be obtained as

$$\omega = \varepsilon_g^{-2.7} \tag{15}$$

In a similar manner, we can calculate the correction factors based on the EMMS approach and that based on Ergun equation.

Fig. 2 illustrates the variation of correction factors with voidage. It can be observed that the correction factors calculated from the EMMS approach are much lower than that from Ergun/Wen and Yu correlations, which is in reasonable agreement with the conclusions from experimental results such as those of Gunn and Malik [20] and Mueller and Reh [21], i.e., the drag coefficient decreases dramatically due to the formation of clusters. Fig. 2 shows further that, at the left side of the curve calculated from the EMMS model, with decreasing voidage, the correction factor curve first increases gradually, then rises abruptly at some turning point to approach the correction factor of Ergun equation. The turning point, as discussed in detail in our previous work [17], corresponds to the abrupt change of structure parameters, reflecting the tendency for gas–solid systems to turn to be homogeneous. At the right side of the curve, with increasing voidage, the correction factor first decreases gradually, then increases and approach to unity, i.e., the correction factor for individual particles. This variation trend is similar to the discussion of Matsen [22] by summarizing experimental results: the slip velocity is very nearly the terminal velocity of a single particle when voidage is greater than the maximum voidage (0.9997), rises to a maximum with decreasing voidage, and then decreases steadily with further decreasing voidage. These results show the reasonableness of the EMMS approach in describing the relationship between the drag coefficient and structure parameters. Recently an attempt has also been made to improve the drag correlation by using the EMMS approach by Xiao et al. [23].

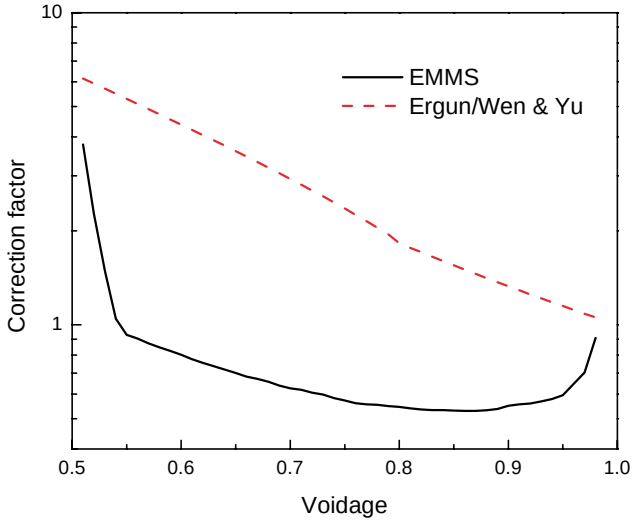

Fig. 2. Comparison of correction factors for drag coefficients (FCC/air: $d_p = 54\,\mu m$, $\rho_p = 930\,kg\,m^{-3}$, $U_g = 1.52\,m\,s^{-1}$, $G_s = 14.3\,kg\,m^{-2}\,s^{-1}$).

If this approach were directly applied to each local control volume, the computational process involving two layers of iteration would require enormous computational cost beyond the current computer capacity. In order to facilitate the application of this approach to the two-fluid model, we assumed that the voidage of dense phase is a constant, and the functions of correction factor vs. voidage correlated from the calculation results of the whole bed can be approximately extended to each local control volume, so the drag coefficient for each control volume can be calculated from the correction factor, the local voidage and the local slip velocity by Eqs. (13) and (14). It should be pointed out that such simplification produces a steeper curve than that in Fig. 2, leading to a much more reduction in drag coefficient when voidage is greater than 0.8. For the case of our simulation ($U_g = 1.52\,m\,s^{-1}$, $G_s = 14.3\,kg\,m^{-2}\,s^{-1}$), the functions of correction factors vs. voidage were correlated as follows:

$$\omega = -0.5760 + \frac{0.0214}{4(\varepsilon_g - 0.7463)^2 + 0.0044} \quad (0.74 \le \varepsilon_g \le 0.82) \tag{16}$$

$$\omega = -0.0101 + \frac{0.0038}{4(\varepsilon_g - 0.7789)^2 + 0.0040} \quad (0.82 \le \varepsilon_g \le 0.97) \tag{17}$$

$$\omega = -31.8295 + 32.8295\varepsilon_g \quad (\varepsilon_g > 0.97) \tag{18}$$

3. Integration of the two-fluid model with the EMMS approach

3.1. Governing equations

The governing equations employed in the two-fluid model include the conservative equations and constitutive

correlations for solid stress and interfacial drag coefficient, as shown below:

- Mass conservative equations for phases ($k = g, p$):

$$\frac{\partial}{\partial t}(\varepsilon_k \rho_k) + \nabla \cdot (\varepsilon_k \rho_k \overline{u}_k) = 0 \tag{19}$$

- Momentum conservative equations for phases ($k = g, p$; $l = p, g$):

$$\frac{\partial}{\partial t}(\varepsilon_k \rho_k \overline{u}_k) + \nabla \cdot (\varepsilon_k \rho_k \overline{u}_k \overline{u}_k) = -\varepsilon_k \nabla p_k + \nabla \cdot \overline{\overline{\tau}}_k - \beta(\overline{u}_k - \overline{u}_k) + \varepsilon_k \rho_k \overline{g} \tag{20}$$

- Gas phase stress:

$$\overline{\overline{\tau}}_g = \varepsilon_g \mu_g \{[\nabla \overline{u}_g + (\nabla \overline{u}_g)^T] - \tfrac{2}{3}(\nabla \cdot \overline{u}_g)\overline{\overline{I}}\} \tag{21}$$

- Solid phase stress:

$$\overline{\overline{\tau}}_p = p_p \overline{\overline{I}} + \varepsilon_p \mu_p \{[\nabla \overline{u}_p + (\nabla \overline{u}_p)^T] - \tfrac{2}{3}(\nabla \cdot \overline{u}_p)\overline{\overline{I}}\} \tag{22}$$

- Solid pressure

$$p_p = 10^{-8.686\varepsilon_g + 6.385} \nabla \varepsilon_p \tag{23}$$

- Solid viscosity:

$$\mu_p = 0.5 \varepsilon_p \tag{24}$$

- Drag coefficient (model A):

$$\text{Ergun}: \quad \beta = 150 \frac{(1-\varepsilon_g)^2 \mu_g}{\varepsilon_g d_p^2} + 1.75 \frac{(1-\varepsilon_g)\rho_g |\overline{u}_g - \overline{u}_p|}{d_p} \quad (\varepsilon_g < 0.80) \tag{25}$$

$$\text{Wen and Yu}: \quad \beta = \frac{3}{4} \frac{(1-\varepsilon_g)\varepsilon_g}{d_p} \rho_g |\overline{u}_g - \overline{u}_p| C_{D0} \varepsilon_g^{-2.7} \quad (\varepsilon_g \geq 0.80) \tag{26}$$

- Drag coefficient (model B):

$$\text{Ergun}: \quad \beta = 150 \frac{(1-\varepsilon_g)^2 \mu_g}{\varepsilon_g d_p^2} + 1.75 \frac{(1-\varepsilon_g)\rho_g |\overline{u}_g - \overline{u}_p|}{d_p} \quad (\varepsilon_g < 0.74) \tag{27}$$

$$\text{EMMS}: \quad \beta = \frac{3}{4} \frac{(1-\varepsilon_g)\varepsilon_g}{d_p} \rho_g |\overline{u}_g - \overline{u}_p| C_{D0} \omega \quad (\varepsilon_g \geq 0.74) \tag{28}$$

The empirical correlations are used to compute the solid stress in our simulation for its simplicity. Two kinds of models are employed to calculate the drag coefficient, i.e., model A (Ergun/Wen and Yu) and model B (Ergun/EMMS), as shown in Eqs. (25)–(28). The correction factor in Eq. (28) is calculated from Eqs. (16)–(18) for the

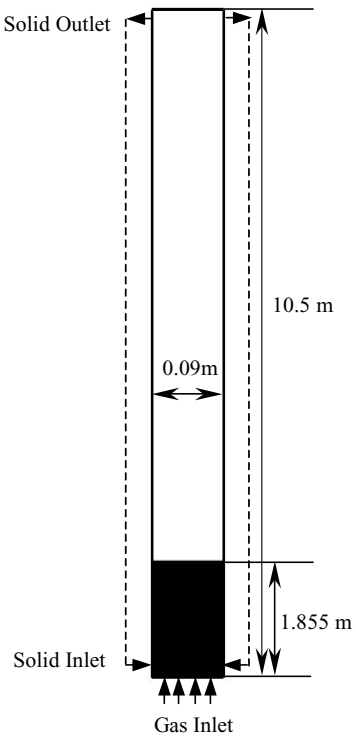

Fig. 3. Schematic drawing of 2D riser.

Table 1
Parameter settings for the simulation

Particle diameter (μm)	54
Particle density (kg m^{-3})	930
Gas velocity (m s^{-1})	1.52
Time interval (s)	5.0×10^{-4}
Grid size, Δx (m)	2.25×10^{-3}
Grid size, Δy (m)	3.5×10^{-2}
Voidage at minimum fluidization	0.4
Maximum voidage for particle aggregating	0.9997
Voidage of dense phase	0.69

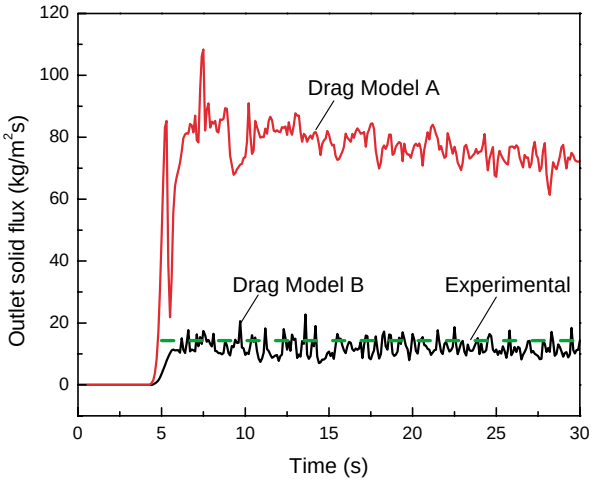

Fig. 4. Comparison between the calculated outlet solid flux and the experimental data.

operating conditions in our calculation ($U_g = 1.52\,m\,s^{-1}$, $G_s = 14.3\,kg\,m^{-2}\,s^{-1}$). At the gas holdup of 0.74, the drag coefficient calculated from the EMMS approach is just beyond that calculated from Ergun equation, so the Ergun equation is employed when the gas hold up is less than 0.74.

3.2. Simulation parameters

Fig. 3 shows the geometry of the riser section of a CFB used in the present simulation. The inlet and the outlet for solids were located at the two sides of riser in the 2D simulation, neglecting the effect of real geometry in 3D experiment.

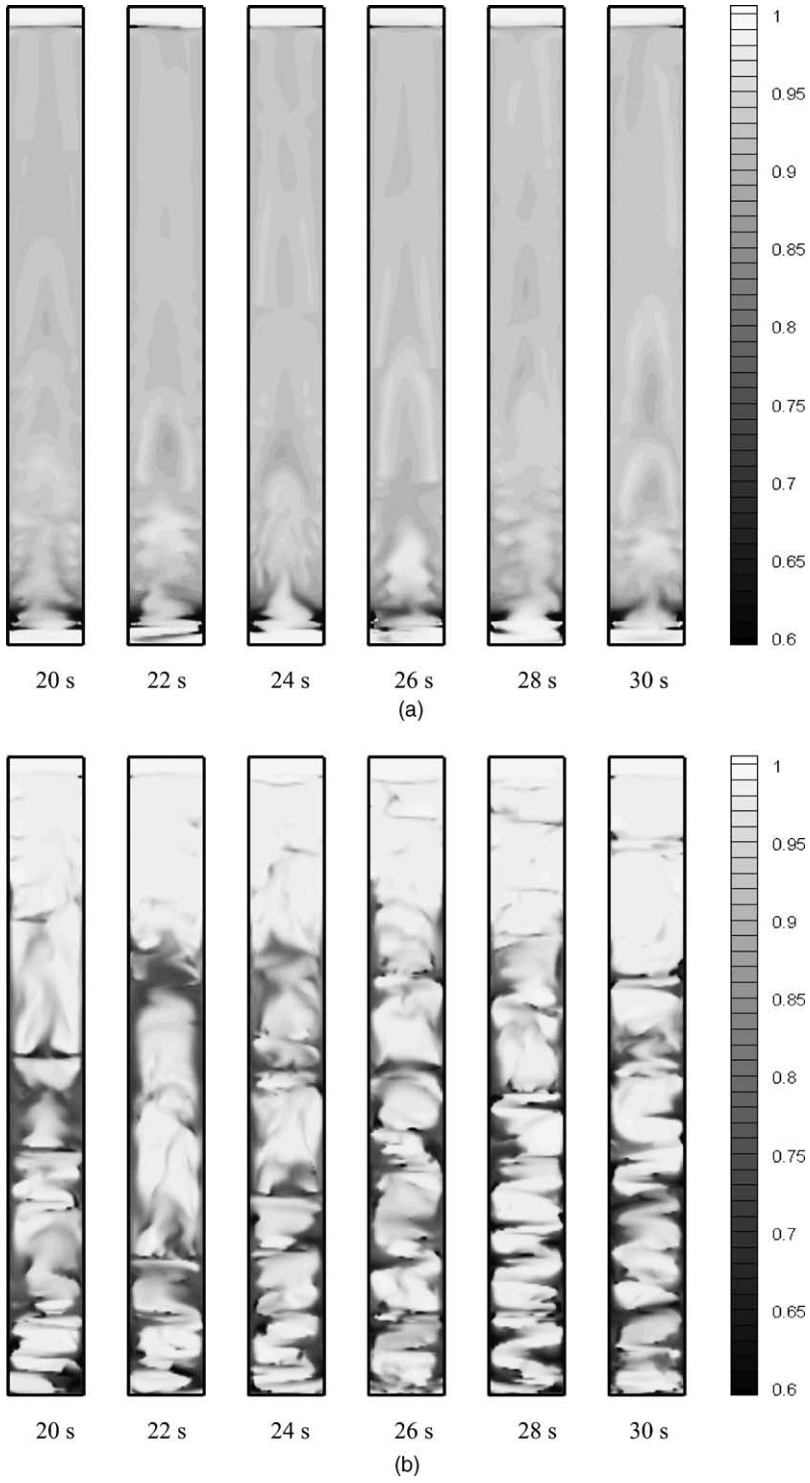

Fig. 5. Snapshot of voidage distribution: (a) drag model A; (b) drag model B.

At the bottom inlet only the gas velocity was specified. Just as the measurement for solid flow rate in experiments, the solid flow rate at the outlet was checked dynamically, and then fed back into the inlet by forcing the solid flow rate at inlet to change into that of outlet. At the initial time, the solid was stacked up to 1.855 m with voidage set to be 0.5. Since we did not simulate the whole loop of the CFB, the initial height (1.855 m) was evaluated from the axial voidage profile of the experimental results. The simulation was carried out with the commercial CFD software CFX4.4 (AEA Technology), in which the inter-phase slip algorithm (IPSA) of Spalding was used to solve the highly coupled partial differential equations. Uniformly distributed grids were adopted in both the lateral and the axial directions. The wall of the bed was modeled as a no-slip rigid wall for the gas phase and a partially slip wall for the solid phase [24]. The detailed simulation parameters are summarized in Table 1.

4. Results and discussion

4.1. Outlet solid flux

Fig. 4 illustrates the variation of outlet solid flux with time. The fluctuation of outlet solid flux reaches a steady state in 6 s. It can be observed that, for the Wen and Yu/Ergun correlations (drag model A), the average value of outlet solid flux (77.8 $kg\,m^{-2}\,s^{-1}$) greatly exceeds the measurement value of experiments (14.3 $kg\,m^{-2}\,s^{-1}$), apparently due to the over-prediction of drag coefficient. While for the EMMS approach (drag model B), the average value of outlet solid flux (12.1 $kg\,m^{-2}\,s^{-1}$) approximates to the experimental value, indicating the effectiveness of the EMMS approach in improving the simulation accuracy.

4.2. Simulation of clustering phenomena

Fig. 5 illustrates the simulated snapshot of voidage distribution by drag model A and drag model B, respectively. It can be observed that, for the Wen and Yu/Ergun approach (drag model A), the solid concentration of the whole bed is quite dilute, and the overall flow structure seems rather homogeneous; while for the EMMS approach (drag model B), the gas–solid system exhibits a more heterogeneous structure, with particle clusters forming and dissolving dynamically. Clusters can be observed to fall along the wall, stack together and then protrude from the wall, while particles are dynamically squeezed out of these clusters and pushed upward by the up-flowing gas, and then these particles further aggregate into strands at an upper section of the bed.

This prediction can be further illustrated in Fig. 6(a) and (b), showing, respectively, the simulated U-shaped clusters and the corresponding solid flow field in a vertical section of the riser (height: 5.0–7.0 m). Clearly observed is the motion of particles into and out of the clusters, viz. descending particles near wall change their motions toward the radial direction, and then are entrained upward by the gas, re-gathering to form strands at an upper section of the riser, as shown in Fig. 6(c) (height: 5.0–10.5 m). These predictions are similar to experimental results such as those of Rhodes et al. [25] that at the interface between the upper dilute region and the lower dense region, the predominant motion is radially inwards and consequently solids are fed from the annulus to the core.

It is interesting to see that, by considering the structure effect on drag coefficient, the cluster behavior at meso-scale can be predicted. The mechanisms of the cluster formation, which may involve gas–particle, particle–particle and particle–wall interactions, are too complex to be well

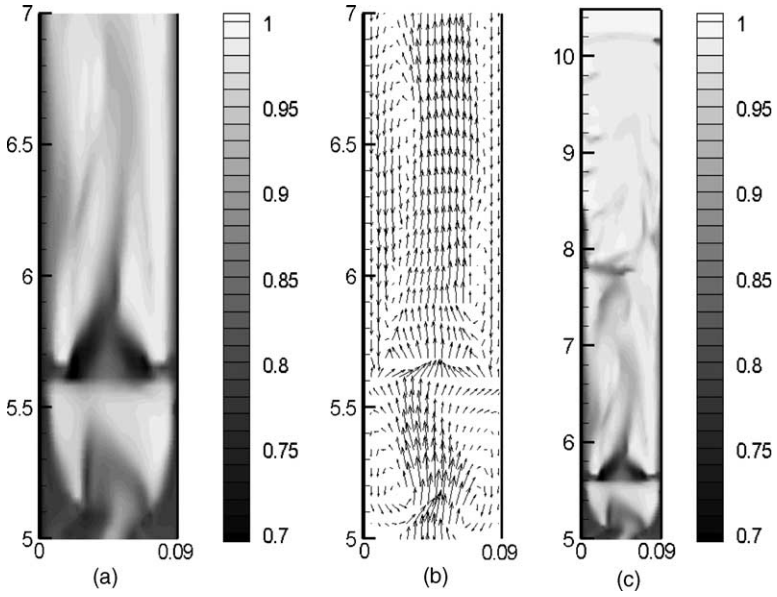

Fig. 6. Sectioned snapshot of cluster formation: (a) voidage profile (no. 20 s, 5.0–7.0 m); (b) solid velocity (no. 20 s, 5.0–7.0 m); (c) voidage profile (no. 20 s, 5.0–10.5 m).

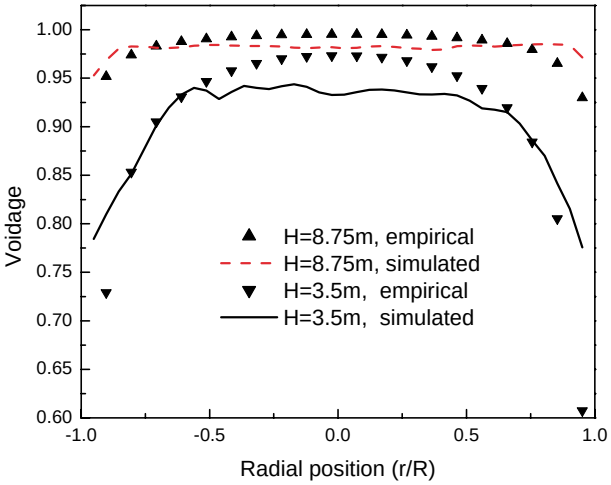

Fig. 7. Radial voidage distribution.

understood. Our simulation results demonstrate that the reduction in drag coefficient is at least an important factor for the simulation of cluster formation, although the underlying mechanisms need further exploration. Since the simulation is still carried out with the coarse grid resolution, the simulated clusters near wall may represent the group behavior of real clusters smaller than the grid size. The high-resolution 3D simulation suggested by Zhang and VanderHeyden [26] shows also the ability of capturing meso-scale structure in spite of its enormous computational cost.

4.3. Radial voidage profile

Fig. 7 shows the comparison of voidage profile in the radial direction between the simulation results (drag model B) and the experimental correlations proposed by Tung et al. [27]. Predicted profiles were drawn from the time-averaged values over the period 20–30 s. The coexistence of a dense annulus and dilute core can be easily recognized, and the radial profile in the top region seems rather flat compared with that in the bottom region. The computed results are in good agreement with empirical correlations in the annulus region, but under-predict the voidage in the core region.

4.4. Axial voidage profile

Fig. 8 shows the comparison of voidage profile in the axial direction between the simulated (drag model B) and the experimental results of Li and Kwauk [19]. Predicted profiles were again drawn from the time-averaged values over the period 20–30 s. The predicted sigmoid distribution of voidage in the axial direction is in reasonable agreement with experimental results, and the deviation may be due to the inaccurate evaluation of solid inventory in the riser at the initial time, and the unrealistic setup of inlet and outlet boundary conditions in the 2D simulation.

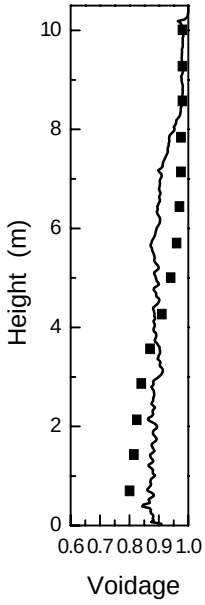

Fig. 8. Axial voidage distribution.

4.5. Velocity distribution

Figs. 9 and 10 show the time-averaged value of simulated solid and gas axial velocities, respectively. At the height of 3.5 m, the core–annulus structure is observed by showing that the solid and gas velocities in the core region are upward and much higher than that in the annulus region, while solid and gas velocities near wall are downward, and this may lead to the so-called backmixing behavior found in experimental research [28]. At the height of 8.75 m, the time-averaged solid and gas velocities near wall change positive, and the radial profile of gas velocity seems much flatter due to the less solid concentration in this region.

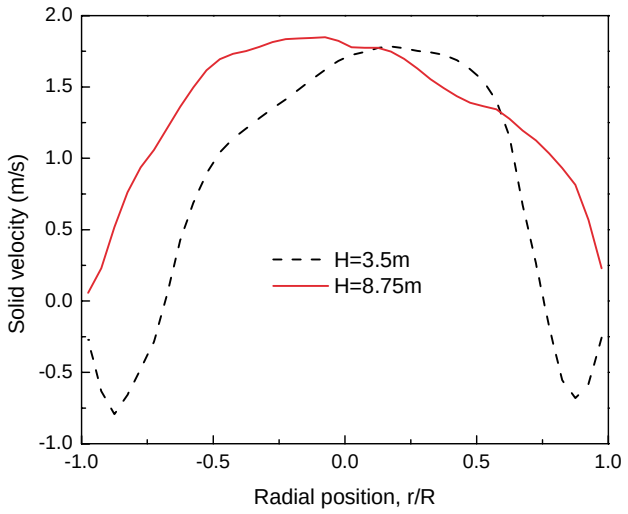

Fig. 9. Solid velocity profiles.

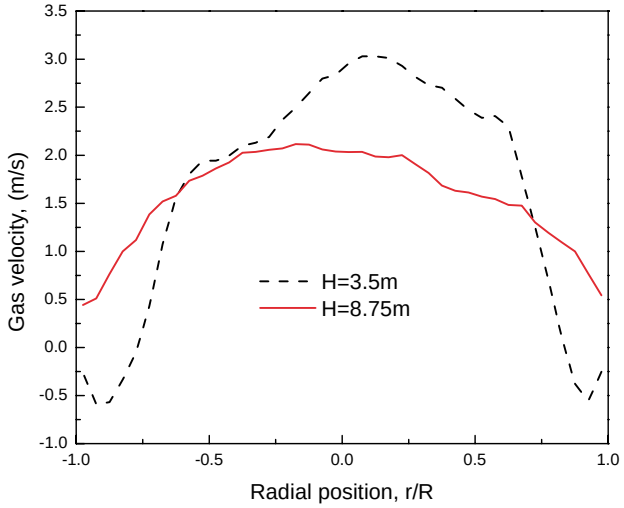

Fig. 10. Gas velocity profiles.

5. Conclusions

Drag coefficient is of crucial importance for the simulation of the heterogeneous gas–solid flow, and its variation is strongly dependent on local structure parameters. However, drag correlations employed in current two-fluid models are derived from experimental results of homogeneous systems without consideration of local heterogeneous structure, and therefore, it is suspected that those drag correlations are capable of reflecting the real mechanisms of gas–solid interactions at the scale of each local control volume.

A feasible approach should correlate the drag coefficient for a control volume with its local structure parameters. The so-called EMMS model seems to be such an approach that the heterogeneous structure is resolved into the dense cluster phase and the dilute phase, and the corresponding gas–solid interactions are resolved into that inside the dense phase and dilute phase, and that between clusters and the surrounding dilute broth. Extending this thought to each local control volume, the EMMS model is in this study adapted to investigate the variations of drag coefficient with structure parameters. Their relationships are established by a set of non-linear equations, and the derived drag correlations are further incorporated into the two-fluid model.

Simulation results show that the drag coefficient calculated from the EMMS model is much lower than that from the Wen and Yu/Ergun correlations, which is in reasonable agreement with the commonly accepted conclusions from experiments. For the Wen and Yu/Ergun correlations, the simulated flow structure is rather dilute and homogeneous, and the outlet solid flux is much higher than the experimental value, apparently due to the over-prediction of drag coefficient. For the EMMS approach, the simulated flow structure is heterogeneous, and the cluster behaviors are captured by showing the course of particle motion, i.e., descending particles near the wall stack together to form clusters; some of them are squeezed out of the radial clusters protrusion and pushed upward by the up-flowing gas, aggregating into strands at the upper section of the riser. The simulated voidage profiles in radial and axial directions, and axial velocities of solid and gas show the formation of core–annulus structure, and are in reasonable agreement with the correlations from experimental results.

These simulation results demonstrate the reasonableness of the EMMS approach in resolving the heterogeneous structure and describing the dependence of drag coefficient on structure parameters, suggesting the feasibility of this approach to be used as a sub-grid closure law for drag coefficient.

Acknowledgements

The authors would like to express their gratitude to Prof. Mooson Kwauk for his encouragement and valuable suggestions to this work. The financial support from the National Natural Science Foundation of China (nos. 90210034, 20221603) and the National Key Program for Developing Basic Sciences of China (no. G1999022103) is also gratefully acknowledged.

References

[1] J. Li, M. Kwauk, Exploring complex systems in chemical engineering—the multi-scale methodology, Chem. Eng. Sci. 58 (2003) 521–535.
[2] T.B. Anderson, R.A. Jackson, A fluid mechanical description of fluidized beds, Ind. Eng. Chem. Fundam. 6 (1967) 527–539.
[3] D. Gidaspow, Hydrodynamics of fluidization and heat transfer: supercomputer modeling, Appl. Mech. Rev. 39 (1) (1986) 1–23.
[4] J.A.M. Kuipers, K.J. Van Duin, F.P.H. Van Beckum, W.P.M. Van Swaaij, A numerical model of gas-fluidized beds, Chem. Eng. Sci. 47 (1992) 1913–1924.
[5] B. Sun, D. Gidaspow, Computation of circulating fluidized-bed riser flow for the fluidization VIII benchmark test, Ind. Eng. Chem. Res. 38 (1999) 787–792.
[6] S. Chapman, T.G. Cowling, The Mathematical Theory of Non-uniform Gases, Cambridge University Press, Cambridge, 1970.
[7] J.L. Sinclair, R. Jackson, Gas–particle flow in a vertical pipe with particle–particle interactions, AIChE J. 35 (1989) 1473–1496.
[8] D. Gidaspow, Multiphase Flow and Fluidization: Continuum and Kinetic Theory Description, Academic Press, Boston, 1994.
[9] C.Y. Wen, Y.H. Yu, Mechanics of fluidization, Chem. Eng. Prog. Symp. Ser. 62 (62) (1966) 100–111.
[10] S. Ergun, Fluid flow through packed columns, Chem. Eng. Prog. 48 (1952) 89–94.
[11] J. Li, C. Cheng, Z. Zhang, J. Yuan, A. Nemet, F.N. Fett, The EMMS model—its application, development and updated concepts, Chem. Eng. Sci. 54 (22) (1999) 5409–5425.
[12] J. Li, A. Chen, Z. Yan, G. Xu, X. Zhang, Particle–fluid contacting in circulating fluidized beds, in: A.A. Avidan (Ed.), Preprint Volume for Circulating Fluidized Beds IV, AIChE, Somerset, 1993, pp. 49–54.
[13] J. Li, L. Wen, W. Ge, H. Cui, J. Ren, Dissipative structure in concurrent-up gas–solid flow, Chem. Eng. Sci. 53 (19) (1998) 3367–3379.
[14] T.J. O'Brien, M. Syamlal, Particle cluster effects in the numerical simulation of a circulating fluidized bed, in: A.A. Avidan (Ed.), Preprint Volume for Circulating Fluidized Beds IV, AIChE, Somerset, 1993, pp. 430–435.

[15] H. Qi, C. You, A. Boemer, U. Renz, Eulerian simulation of gas–solid two-phase flow in a CFB-riser under consideration of cluster effects, in: D. Xu, S. Mori (Eds.), Fluidization 2000: Science and Technology, Xi'an Publishing House, Xi'an, 2000, pp. 231–237.
[16] K. Agrawal, P.N. Loezos, M. Syamlal, S. Sundaresan, The role of meso-scale structures in rapid gas–solid flows, J. Fluid Mech. 445 (2001) 151–185.
[17] N. Yang, W. Wang, W. Ge, J. Li, Analysis of flow structure and calculation of drag coefficient for concurrent-up gas–solid flow, Chin. J. Chem. Eng. 11 (1) (2003) 79–84.
[18] N. Yang, W. Wang, W. Ge, J. Li, Choosing structure-dependent drag coefficient in modeling gas-solid two-phase-flow, China Particuology 1 (1) (2003) 38–41.
[19] J. Li, M. Kwauk, Particle–fluid Two-phase Flow—The Energy-minimization Multi-scale Model, Metallurgy Industry Press, Beijing, 1994.
[20] D.J. Gunn, A.A. Malik, The structure of fluidized beds in particulate fluidization, in: A.A. Dringkenburg (Ed.), Proceedings of the International Symposium on Fluidization, Netherlands University Press, Eindhoven, 1967, pp. 52–65.
[21] P. Mueller, L. Reh, Particle drag and pressure drop in a accelerated gas–solid flow, in: A.A. Avidan (Ed.), Preprint Volume for Circulating Fluidized Beds IV, AIChE, Somerset, 1993, pp. 193–198.
[22] J.M. Matsen, Mechanisms of choking and entrainment, Powder Technol. 32 (1982) 21–33.
[23] H.T. Xiao, H.Y. Qi, C.F. You, X.C. Xu, Theoretical model of drag between gas and solid phase, J. Chem. Ind. Eng. 54 (2003) 311–315 (in Chinese).
[24] J. Ding, D. Gidaspow, A bubbling fluidization model using kinetic theory of granular flow, AIChE J. 36 (4) (1990) 523–538.
[25] M.J. Rhodes, M. Sollaart, X.S. Wang, Flow structure in a fast fluid bed, Powder Technol. 99 (1998) 194–200.
[26] D.Z. Zhang, W.B. VanderHeyden, High-resolution three-dimensional numerical simulation of a circulating fluidized bed, Powder Technol. 116 (2001) 133–141.
[27] Y. Tung, J. Li, M. Kwauk, Radial voidage profiles in a fast fluidized bed, in: M. Kwauk, D. Kunii (Eds.), Fluidization'88: Science and Technology, Science Press, Beijing, 1988, pp. 139–145.
[28] J. Li, H. Weinstein, An experimental comparison of gas backmixing in fluidized beds across the regime spectrum, Chem. Eng. Sci. 44 (1989) 1697–1705.